is lower than the global average but still greater than observed for the United States and Europe.

Emissions of $CH_3CCl_3$ (with respect to CFC-11) are clearly different from the three continents: the western United States is a factor of 1.3 above the global mean, and Australia a factor of 2 below. A balance of sources from the United States and western Europe could maintain the $CH_3CCl_3$ global budget.

Carbon tetrachloride shows a large European source (with respect to CFC-11) which is still less than estimates for the mean global source. As the United States and Australia seem to contribute lesser relative amounts of $CCl_4$, I conclude that additional sources may be required, perhaps also associated with the missing CFC-12. The primary pollution events at Adrigole show a $CCl_4$:CFC-11 ratio typical of the other continents (~0.15). The larger sources of $CCl_4$ are associated with high coherence at time lags or more than 4 days, enough time for air to have crossed the European continent.

Nitrous oxide variability at Adrigole shows a component clearly correlated with halocarbon pollution events. This relationship is consistent with an industrial source of $N_2O$ from combustion of fuel nitrogen[13,14] which is spatially associated with halocarbon releases. If scaled to global CFC-11 emissions, the magnitude of this source is $\sim 3 \times 10^{12}$ g(N) $yr^{-1}$, is equivalent to the observed annual increase in $N_2O$, and accounts for ~25% of the current global emissions[7].

Concurrent atmospheric measurements, made at a frequency greater than one per day, provide valuable information on the location and magnitude of sources for many trace gases of both natural and anthropogenic origin. These data permit integration of emissions over large areas and present critical tests for the synoptic-scale transport of trace gases in three-dimensional models. Locations of observing stations near, but not in the middle of suspected sources would allow determination of baseline trends[17] as well as emissions.

This research was supported by NSF grant ATM-81-17009 and NASA grant NAGW-359. I gratefully acknowledge availability of the atmospheric measurements from the ALE team and helpful discussions with S. Wofsy and R. Prinn.

Received 28 March; accepted 10 July 1985.

1. Keeling, C. D. *et al. Tellus* **28**, 538-551 (1976).
2. Dianov-Klokov, V. I. & Yurganov, L. N. *Tellus* **33**, 262-273 (1981).
3. Rasmussen, R. A. & Khalil, M. A. K. *Atmos. Envir.* **15**, 883-886 (1981).
4. Ehhalt, D. H., Zander, R. J. & Lamontagne, R. A. *J. geophys. Res.* **88**, 8442-8446 (1983).
5. Craig, H. & Chou, C. C. *Geophys. Res. Lett.* **9**, 477-481 (1982).
6. Khalil, M. A. K. & Rasmussen, R. A. *Science* **224**, 54-56 (1984).
7. Weiss, R. F. *J. geophys. Res.* **86**, 7185-7196 (1981).
8. Fraser, P. J., Hyson, P., Enting, I. G. & Perman, G. I. *Nature* **302**, 692-695 (1983).
9. Prinn, R. G. *et al. J. geophys. Res.* **88**, 8353-8441 (1983).
10. *Causes and Effects of Changes in Stratospheric Ozone: Update 1983* (National Research Council, National Academy, Washington DC, 1984).
11. Prather, M. J., McElroy, M. B. & Wofsy, S. C. *Nature* **312**, 227-231 (1984).
12. *Production, Sales and Calculated Release of CFC-11 and CFC-12 Through 1982* (Chemical Manufacturers Association, Washington DC, 1983).
13. Weiss, R. F. & Craig, H. *Geophys. Res. Lett.* **3**, 751-753 (1976).
14. Pierotti, D. & Rasmussen, R. A. *Geophys. Res. Lett.* **3**, 265-267 (1976).
15. Blake, D. R., Woo, V. H., Tyler, S. C. & Rowland, F. S. *Geophys. Res. Lett.* **11**, 1211-1214 (1984).
16. Pack, D. H., Lovelock, J. E., Cotton, G. & Curthoys, C. *Atmos. Envir.* **11**, 329-344 (1977).
17. Graedel, T. E. & McRae, J. E. *Geophys. Res. Lett.* **11**, 977-979 (1980).

# Segmentation of mid-ocean ridges

**Hans Schouten*, Kim D. Klitgord† & John A. Whitehead***

* Woods Hole Oceanographic Institution, Woods Hole, Massachusetts 02543, USA
† US Geological Survey, Woods Hole, Massachusetts 02543, USA

*Studies of mid-ocean ridges in the Pacific and Atlantic oceans show that the volcanism that forms the oceanic crust along the spreading-plate boundaries is concentrated at regular intervals related to spreading rate. This observation and a new calculation for a Rayleigh–Taylor type of gravitational instability of a partially molten mantle region growing under spreading centres yield reasonable estimates of upper mantle viscosities.*

SEGMENTATION of mid-ocean ridges seems to be a global phenomenon. Mid-ocean ridges are the spreading boundaries or spreading centres between lithospheric plates where new oceanic crust and lithosphere is created at rates of 10–200 km $Myr^{-1}$. Although continuous overall, mid-ocean ridges are cut by many transform zones and associated fracture zones that offset the spreading centre by distances up to several hundred kilometres (Fig. 1). These fracture zones divide the ridges into a series of relatively straight segments with lengths of several tens to several hundreds of kilometres. As more high-resolution geophysical surveys of mid-ocean ridges are becoming available in the world's ocean basins, an even more orderly pattern of the sea floor is emerging. This pattern indicates that the boundaries between the spreading plates have a fairly rigorous cellular structure on a 30–80 km length scale.

The spreading centre cells seem to be the primary feature of mid-ocean ridges; they suggest a three-dimensional, rather than two-dimensional, process of magmatism and crustal accretion spaced evenly along the present spreading boundary. Magnetic studies of older oceanic crust suggest relatively stable and even segmentation of plate boundaries in the past on the same length scale[1,2]. Seismic studies indicate that oceanic crust with normal seismic structure is formed in the spreading centre cells and that between the cells, thinner crust and other structural anomalies characteristic of fracture zones are formed, regardless of the spatial offset between the spreading centres[3–7].

The transition zones or transform zones between centres on the active mid-ocean ridges manifest themselves in variable and complex ways. Where large offsets exist between the centres, well-defined, predictable transform fault zones provide the continuity and stability of the active plate boundary between the spreading centres on either side of the transform. Where no offsets are apparent between the spreading centre cells, the transition zones between centres are complex, variable and inherently unstable on an approximate length scale of 10 km and timescale of $10^5$–$10^6$ yr (refs 8, 9), but they are apparently stable when observed on longer length- and timescales[1–3,7].

The apparent stability in space and time on the longer length- and timescales of a regular segmentation of mid-ocean ridges has been attributed by Whitehead, Dick and Schouten[10] to a Rayleigh–Taylor type of gravitational instability of a partially molten mantle region beneath spreading centres. In this model, the wavelength of the instability controls the aggregation and diapiric ascent of mantle melt (magma) at regular intervals along the boundary between two spreading plates.

Here we use the results of high-resolution geophysical surveys of mid-ocean ridges and determine the length scales of segmentation as a function of spreading rate. We use a modification of

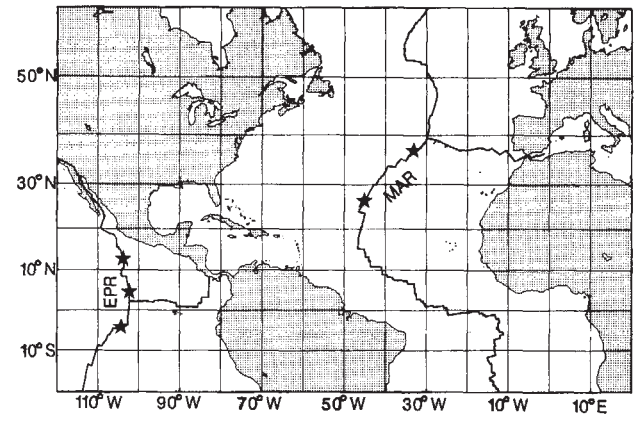


**Fig. 1** Atlantic and Pacific spreading centres and transform zones which form the boundaries between the spreading lithospheric plates. Stars denote the location of five high-resolution surveys of the Mid-Atlantic Ridge (MAR) and East Pacific Rise (EPR) discussed in this article.

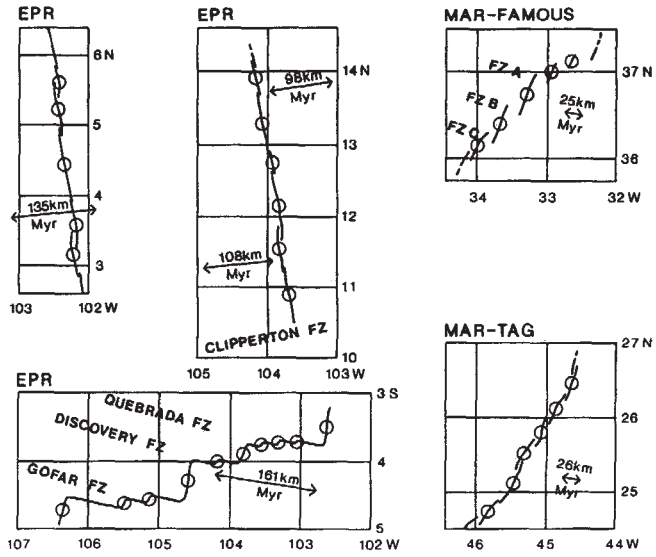


**Fig. 2** Segmentation of seafloor spreading centres from high-resolution geophysical data on EPR and MAR. Lines denote neovolcanic zones inferred from ridge-axis topographical highs (on fast-spreading EPR) and deeps (on slow-spreading MAR). EPR 3°–6° N after Lonsdale[14] (multi-narrow-beam bathymetry data); EPT 10°–14° N after Macdonald and Fox[8] and Macdonald *et al.*[9] (multi-narrow-beam bathymetry data); MAR 25°–27° N modified from Rona *et al.*[16] and Rona and Gray[17] (single narrow-beam bathymetry data, average track spacing 7 nm); MAR 35°–37° N modified from Ramberg and van Andel[15] (multi-narrow-beam and single-beam bathymetry data). The heavy line in EPR 5°–3° S denotes the Pacific–Nazca plate boundary after Searle[30] (GLORIA long-range side-scan sonar data). Open circles, placed at midpoints of the spreading-centre segments, denote hypothetical centres of magmatic activity. Arrows indicate total seafloor spreading (after ref. 38). Average spacing of these centres as a function of effective spreading rate is shown in Fig. 3. We postulate that the fairly even spacing of these centres can be attributed to a Rayleigh–Taylor type of gravitational instability of a lower density and viscosity region of high-melt content collecting at the base of melt-depleted mantle at some depth beneath the spreading plate boundary. The reduced distance between centres in EPR 5°–3° S can be attributed to reduced rate of melt production per unit length along this oblique section of the spreading plate boundary; the average effective spreading rate on this oblique boundary is of the order of 75 km $Myr^{-1}$ or less than half the spreading rate at this location.

a theory by Howard[11] for Rayleigh–Benard convection to predict length- and timescales of magmatic activity as a function of spreading rate. We show that observed length- and timescales of magmatic activity on mid-ocean ridges predict reasonable upper mantle viscosities, suggesting that the chosen length- and timescales and the proposed theory are appropriate. This provides additional supporting evidence for the mechanism for magmatic accretion under spreading centres proposed by Whitehead *et al.*[10] and for the predictability and inherent stability of length- and timescales of magmatism and crustal accretion on past and present-day mid-ocean ridges.

## Spreading centre segmentation

A detailed SEABEAM investigation of the East Pacific Rise (EPR in Fig. 1), which provided continuous along-strike coverage of the rise-axis bathymetry between 8° N and 18° N, revealed that the continuity of a 550-km-long spreading-centre segment between the Clipperton Fracture Zone (10° N) and the Orozco Fracture Zone (15° N) was disrupted in at least six locations by a volcano-tectonic geometry characterized by two overlapping (en-echelon) neovolcanic zones enclosing an elongate depression[8,9] (EPR 10°–14° N in Fig. 2). The existence of similar disruptions of the southern East Pacific Rise axis between 20° S and 7° N has been reported by Lonsdale[12–14] (EPR 3°–6° N in Fig. 2). Schouten and Klitgord[2] have argued that these geometries are the morphological expression on fast spreading ridges of 'zero-offset' transform zones between spreading-centre cells which have been stationary features on the EPR spreading axis for at least 5 Myr.

The segmentation of the mid-Atlantic Ridge (MAR in Fig. 1) has been suggested by interpretations of high-resolution surveys in the FAMOUS area[15] (MAR 36°–37° N in Fig. 2) and in the TAG area[16,17] (MAR 25°–27° N in Fig. 2) which indicate a spreading-centre spacing of the order of 40 and 45 km, respectively. Any spatial offset between two rift valleys translates into a significant age offset on this slowly spreading (~25 km $Myr^{-1}$) plate boundary. Age offset rather than spatial offset seems to characterize the anomalous great depths found at ridge/transform intersections[18], causing significant disruptions in the rift-valley bathymetry. If we interpret each rift-valley segment bounded by anomalous depths as a spreading-centre cell, then bathymetry between the Kane Fracture Zone at 24° N and the Azores triple junction of the North American, African and European plates at 38° N would give an estimated distance between cell centres of 50 ± 10 km, which is in agreement with the high-resolution observations in FAMOUS and TAG. On the faster spreading EPR we interpret the disruptions of the neovolcanic zones shown in Fig. 2 as the boundaries between spreading-centre cells, indicating a fairly even spreading-centre spacing of the order of 65 km.

## Three-dimensional magmatic accretion

Submersible observations and bottom camera surveys at spreading centre/transform zone intersections indicate an apparent reduction of magmatic activity towards the transform zone regardless of transform offset (see refs 18, 19). Near-bottom observations of the Galapagos Rift at 86° W have shown clear along-strike variations in volcanism, structure and hydrothermal activity along a 30-km section of a 250-km long spreading-centre segment, suggesting a three-dimensional rather than two-dimensional process of magmatism and crustal accretion[20]. Similar observations of the along-strike variability of axial processes on the EPR near 20° S, 13° N and 21° N and on the Juan de Fuca Ridge support a three-dimensional model of magmatic accretion in seafloor spreading centres[21,22]

## Segmented magmatic accretion

The cellular structure of the boundaries between spreading plates is one of the arguments used by Whitehead *et al.*[10] and Crane[23] to support a new model of magmatic accretion under spreading centres. In this model, the mechanism that controls the segmentation of mid-ocean ridges is attributed to a Rayleigh–

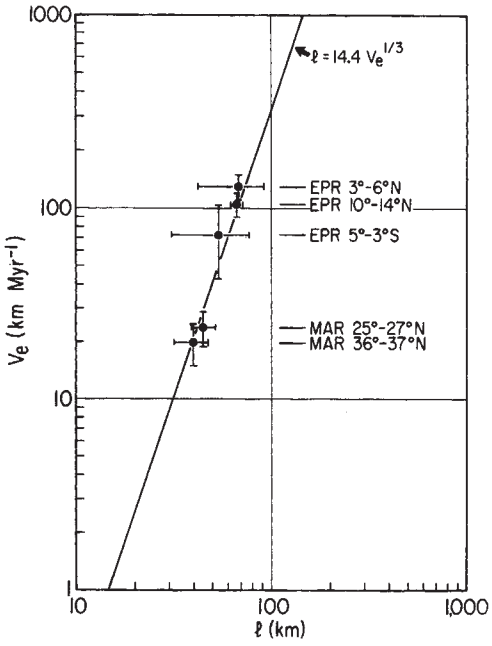


**Fig. 3** Spacing ($l$) of hypothetical centres of magmatic activity (from Fig. 2) against effective spreading rate $v_e$ (error bars are ±1 s.d.) and a best-fit model for the proposed relationship where $l \propto v_e^{1/3}$, or $l = 14.4\ v_e^{1/3}$. This model predicts an average spreading-centre spacing of 85 km for a 200 km Myr$^{-1}$ spreading rate at 20° S on the EPR.

Taylor type of gravitational instability of a lower viscosity and lower-density partially molten region collecting at the base of melt-depleted mantle at some depth within the asthenosphere rising beneath the spreading-centre axis. The wavelength or spacing of the fastest growing instability of the low-viscosity material is a function of the geometry of that region and of the viscosities of the partially molten region and the surrounding asthenosphere[10,24,25].

Considering that mid-ocean ridge basalts (the mantle melt that has aggregated from a partially molten mantle and risen to the surface to form the oceanic crust) have a rather characteristic and uniform composition throughout the world[26], it is probable that the viscosities of the partially molten region and the surrounding asthenosphere beneath mid-ocean ridges are uniform also, and independent of spreading rate. However, the production of melt, caused by the decompression of the asthenosphere as it rises to fill the gap between two spreading plates, must at least equal production of oceanic crust. If we make a first-order approximation that the thickness of oceanic crust is uniform and independent of spreading rate, then production of melt beneath mid-ocean ridges would be proportional to spreading rate.

The model of Whitehead *et al.*[10] postulated a linearly continuous partially molten region beneath the spreading plate boundary. The width of this region cannot exceed the width of the asthenosphere rising between the spreading lithospheric plates. This width is a function of depth or age as the lithospheric plates thicken with age away from the axis[27,28]. At 25 km depth beneath the spreading axis, where the instability is postulated to occur[10], the width of the asthenosphere between the lithospheric plates is the total spreading rate multiplied by 4 Myr (ref. 27) to 7 Myr (ref. 28). On the fast-spreading EPR (100–200 km Myr$^{-1}$), between Rivera Fracture Zone (18° N) and Eltanin Fracture Zone (57° S), most transform offsets are ≤1 Myr times the spreading rate (comparable with offsets of ≤25 km in the slow-spreading central North Atlantic). These offsets would be insufficient to disrupt the continuity of a partially molten region at 25 km depth beneath the overall spreading boundary. A linearly continuous partially molten region beneath the EPR axis, with its gravitational instability driving the segmentation of this axis, would explain the phenomenon of multiple closely spaced transform zones. The double Orozco Fracture Zone at 15° N (ref. 29) provides the continuity of regular spacing (of the order of 65 km) between centres of magmatic activity along an oblique part of the overall plate boundary. The multiple Quebrada, Discovery and Gofar Fracture Zones near 5° S on the EPR surveyed with GLORIA[30] (EPR 5°–3° S in Fig. 2) suggests a fairly regular spacing between centres of magmatic activity (of the order of 55 km) along a very oblique section of the overall spreading boundary (the trend is ~30° to the spreading direction).

To include the segmentation of oblique plate boundaries in our estimates, we postulate that the average production of melt per unit length along the average boundary is proportional to the effective spreading rate (where effective spreading rate is the component of spreading perpendicular to the regional trend of the spreading plate boundary). A plot of average distance

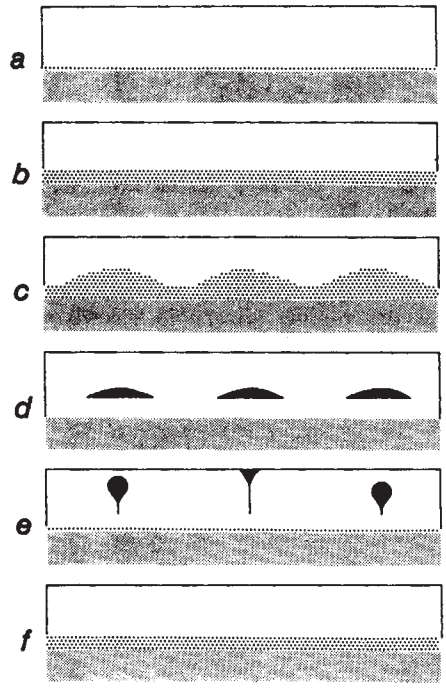


**Fig. 4** Along-axis diagram of the proposed mechanism of magmatic upwelling beneath mid-ocean spreading centres. Fine stipples, parental upper mantle; coarse stipples, partially molten mantle; no stipples, melt-depleted mantle; solid black, aggregated mantle melt (magma). A region of partially molten mantle begins to collect at the base of the depleted mantle in the asthenosphere beneath the spreading axis (*a*). As the volume of this region grows (*b*), the partially molten mantle, which has a lower density and viscosity than the surrounding asthenosphere, develops a gravitational instability with regularly spaced disturbances (*c*). Once the disturbances are established, the very low viscosity melt (magma), which can migrate by porous flow and moves more rapidly than the partially molten region as a whole, concentrates at the tops of the rising disturbances (*d*), after which it rises diapirically (*e*) towards the magma chambers in the oceanic crust above. The partially molten region is depleted of the melt (*d*) and the process will repeat itself as a new region of partially molten mantle begins to grow again at the base of the freshly depleted mantle (*e*, *f*).

between centres of magmatic activity (that is, the centres of spreading-centre segments indicated by circles in Fig. 2) versus effective spreading rate is shown in Fig. 3. The segmentation of mid-ocean ridges would be proportional approximately to one-third power of the effective spreading rate (Fig. 3).

## Rayleigh–Taylor instability

We use a modification of a remarkably simple theory by Howard[11] for Rayleigh-Benard convection (a horizontal layer of fluid heated from below) to predict spacing between centres of magmatic activity as a function of spreading rate. In Howard's theory, the conductive growth of a thermal boundary layer from an initially isothermal state was shown to proceed as an error function. The boundary layer could be next to either the cold top plate or the hot bottom plate. He postulated that the boundary layer would grow until its local Rayleigh number reached a number of 1,000–3,000. Next, a disturbance would grow more rapidly than the conductive boundary layer, and a blob of fluid would detach from the boundary. The boundary layer would be swept free of the boundary and the process would repeat itself as fluid near the boundary began to form a new thermal boundary layer. The calculation led to the correct prediction that heat transport would be proportional to Rayleigh number (dimensionless temperature difference) to the one-third power, a result known to be true both from experiment and by more rigorous and much more complicated theories[11,31,32].

Here we do not have a conductive boundary layer but instead consider a growing horizontal cylindrical body of fluid with relatively low viscosity and density compared with the surrounding liquid. This represents a linear region of relatively high melt content growing in the Earth's mantle below the spreading boundary. To be consistent with uniform formation of oceanic crust, we postulate that the volume of the cylindrical body increases uniformly with time. The diameter of this body will increase proportionally to the square root of time, that is

$$d = \left(\frac{4\,Ut}{\pi}\right)^{1/2} \tag{1}$$

where $U$ is the two-dimensional volumetric production rate of the lower viscosity and density region and $t$ is time. We imagine this is the first part of a cycle in which upwelling mantle develops a linear region of lower viscosity and of density $\rho - \Delta\rho$.

The appropriate gravitational instability for a horizontal cylindrical volume is a modified Rayleigh–Taylor instability[10,25] for which it has been shown that small disturbances will grow exponentially as $\exp(t/\tau)$, where (using equation (1)) the timescale $\tau$ is

$$\tau = \frac{1}{0.153}\frac{\mu_2}{g\Delta\rho}\left(\frac{\pi}{4Ut}\right)^{1/2}\left(\frac{\mu_2}{\mu_1}\right)^{-1/3} \tag{2}$$

Here $\mu_2$ is the viscosity of the surrounding mantle fluid, $\mu_1$ the viscosity of the cylindrical volume of high-melt content and $g$ is the force of gravity. Although this equation is strictly valid only for large values of $\mu_2/\mu_1$, it is quite accurate for values as low as 1.5 or 2. Equation (2) shows that $\tau$ is initially infinite, but that it decreases inversely as the square root of time (that is, diameter). As a modification to Howard's theory, let us assume that as the volume grows, no disturbances will be apparent until a time ($t_c$) of the order of $\tau$ (Marsh[25] advocates a factor of $5\tau$ before protrusions are seen experimentally). Setting $t = t_c = \tau$ in equation (2) and solving for $t_c$, we get

$$t_c = \left[\frac{1}{0.173}\frac{\mu_2}{g\Delta\rho}\left(\frac{1}{U}\right)^{1/2}\left(\frac{\mu_2}{\mu_1}\right)^{-1/3}\right]^{2/3} \tag{3}$$

The wavenumber of fastest growing disturbances for a cylindrical volume is advocated by Marsh[25] to be

$$k_c = \frac{2.15}{d}\left(\frac{\mu_1}{\mu_2}\right)^{1/3} \tag{4}$$

Using equations (1), (3) and (4) and $k_c = 2\pi/\lambda_c$, where $\lambda_c$ is the critical wavelength, we get the following expression for the wavelength of fastest-growing disturbances at critical time $t_c$, that is

$$\lambda_c = \frac{1}{0.169}\,U^{1/3}\left(\frac{\mu_2}{g\Delta\rho}\right)^{1/3}\left(\frac{\mu_2}{\mu_1}\right)^{2/9} \tag{5}$$

We suggest that once disturbances with this spacing are established in the partially molten mantle region, the very low viscosity melt, which can migrate by porous flow[33] would move more rapidly than the partially molten region as a whole and concentrate at the tops of the rising disturbances, after which it would be drawn off through conduits[10] (Fig. 4). The partially molten region would be depleted of the melt and the process would repeat itself as a new region of high-melt content begins to grow at the base of the freshly depleted mantle.

Of special interest will be the product of equations (3) and (5), which reduces to the simple expression

$$\lambda_c t_c = 19.1\,\frac{\mu_2}{g\Delta\rho} \tag{6}$$

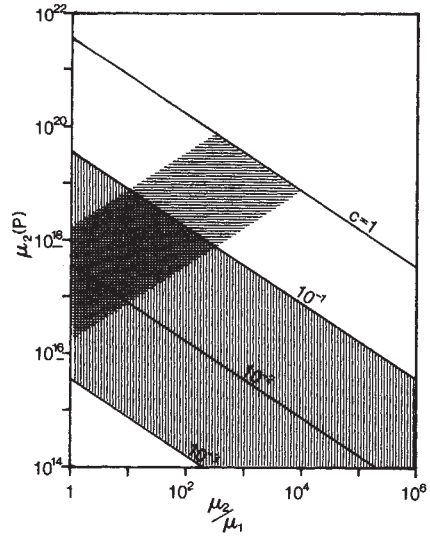


**Fig. 5** Constraints on upper mantle viscosity ($\mu_2$) and the ratio, $\mu_2/\mu_1$, of mantle viscosity to viscosity of the partially molten mantle region ($\mu_1$) under seafloor spreading centres. $c$, Concentration of melt in the partially molten region. Lines of constant $c$ are drawn from equation (9) which relates the wavelength of a Rayleigh–Taylor instability to observed length scales of magmatic activity on mid-ocean ridges. Values of $c > 1$ are impossible, and $(\mu_2/\mu_1) < 1$ is considered to be physically unlikely. Vertical hachures indicate a permissible range of melt concentrations $10^{-1} > c > 10^{-3}$; greater values would result in semi-suspended slurry with too-large values of $\mu_2/\mu_1$; smaller values of $c$ would not result in a sizeable magma genesis. A second constraint (horizontal hachures) arises from the observed time- and length scale of magmatic activity in the central North Atlantic FAMOUS area and from equation (6). The centre of intersecting hachures lies at $\sim\mu_2 = 10^{18}$ P, $(\mu_2/\mu_1) = 10$, $c = 3\%$. The fact that these numbers are reasonable suggests that length- and timescales of magmatic activity on mid-ocean ridges can provide important boundary conditions for models of mantle upwelling under spreading centres.

## Discussion

The most striking property of equation (5) is the dependence of spacing on production rate to the one-third power, which matches the empirical dependence found in Fig. 3 of spreading-centre spacing $l$ on effective spreading rate $v_e$ to approximately the one-third power. We postulate a model of the form of

$$l = Q\,v_e^{1/3} \tag{7}$$

to fit the data in Fig. 3, and choose $Q = 14.4\,\mathrm{km^{2/3}\,Myr^{1/3}}$ as a best fit. We relate the volumetric production rate $U$ of a partially

molten mantle region beneath spreading centres to the three quantities: effective spreading rate, thickness of oceanic crust $T$ and the melt concentration $c$ in the partially molten region. We assume that production of melt equals production of oceanic crust, thus the production rate of the partially molten region is given by

$$U = \frac{v_e T}{c} \tag{8}$$

Equations (5), (7) and (8) can be combined to relate the empirical parameter $Q$ with $\mu_1$, $\mu_2$, $\Delta\rho$, $c$ and $T$. Setting $l = \lambda_c$, we obtain

$$\mu_2 = (0.169\ Q)^3 \frac{cg\Delta\rho}{T}\left(\frac{\mu_2}{\mu_1}\right)^{-2/3} \tag{9}$$

This relationship is illustrated in Fig. 5 with the following numbers for the observed quantities: $Q = 0.98 \times 10^9$ cm$^{2/3}$ s$^{1/3}$, average thickness of oceanic crust (fracture zones included) $T = 5 \times 10^5$ cm and $g = 10^3$ cm s$^{-2}$. It is further assumed that $\Delta\rho$ of the partially molten region is proportional to melt concentration, that is, $\Delta\rho = 0.4\ c$ gm cm$^{-3}$. Thus, our remaining unknowns are $\mu_2$, $\mu_2/\mu_1$ and $c$; lines of constant $c$ are presented in a $\mu_2$, $\mu_2/\mu_1$ plane. Vertical hachures in Fig. 5 indicate a permissible range of melt concentrations $10^{-1} > c > 10^{-3}$. If the postulated dynamics are correct and if the value of $Q$ adopted here predicts the correct spreading-centre spacing on the world's mid-ocean ridges, then Fig. 5 will provide important constraints on the viscosities of the upper mantle and the partially molten region below spreading centres.

An additional physical prediction of the model is the critical time $t_c$, which can be thought of as a timescale of magmatic activity. From equations (3) and (8) it is easy to see that also the frequency $(1/t_c)$ of the process should be proportional to effective spreading rate to the one-third power, predicting a frequency of magmatic activity in the fastest spreading centres (EPR 20° S at 200 km Myr$^{-1}$) that is only a factor of two greater than the frequency of magmatic activity in slow-spreading centres (MAR at 25 km Myr$^{-1}$). Recent near-bottom studies of spreading-centre activity along the EPR axis indicate a frequency of magmatic activity which is only a factor of two or three higher than that of the FAMOUS area and Reykjanes Ridge on the slow-spreading MAR (R. D. Ballard, personal communication) which is consistent with the prediction from our model.

From an interpretation of FAMOUS rift valley geomorphology, Ballard and van Andel[34] estimate a period of magmatic activity of the order of $10^4$ yr. The wavelength of magmatic activity or spreading-centre spacing in this area is 40 km (MAR 36°–37° N in Fig. 2). We use these estimates of period and wavelength from the FAMOUS area with equation (6) to predict upper mantle viscosity $\mu_2$. Taking $t_c = 10^{4\pm0.5}$ yr, $\lambda_c = 40$ km, $g = 10^3$ cm s$^{-2}$ and assuming $\Delta\rho = 0.4\ c$ g cm$^{-3}$ we find from equation (6) that $\mu_2 = 2.64 \times 10^{19\pm0.5}\ c$. This estimate is represented with the horizontal hachures in Fig. 5. The area of intersecting vertical and horizontal hachures in Fig. 5 is a constraint in parameter space which implies that only a low-viscosity contrast ($<10^2$) and a viscosity of upper mantle under spreading centres of $\mu_2 = 10^{18\pm1}$ P are compatible with the theory and the observed length- and timescales of magmatic activity on mid-ocean ridges. The centre of intersecting hachures in Fig. 5 lies at $\sim\mu_2 = 10^{18}$ P, $(\mu_2/\mu_1) = 10$, $c = 3\%$.

These estimates are consistent with some geophysical, petrological and experimental observations. From gravity and models of the median valley on the MAR, Collette *et al.*[35] have estimated a value of $10^{19.5}$ P for the viscosity of upper mantle beneath this plate boundary. Based on petrological studies of Alpine peridotites, Dick and Sinton[36] concluded that dissolution creep may be the dominant mechanism for both deformation and compositional layering in a partially molten upper mantle under spreading centres. Recent hot-pressing experiments by Cooper and Kohlstedt[37] on olivine–basalt assemblages to simulate dissolution creep in a peridotitic upper mantle indicate that the viscosity contrast between melt-free and partially molten mantle would be $>1$ and $<10$. This suggests that the choice of observed length- and timescales of magmatic activity on mid-ocean ridges and the proposed theory are appropriate, and if tighter constraints on these scales and on $\mu_2$, $\mu_1$, $c$ or $\Delta\rho$ could be achieved, a more refined theory (tested carefully by laboratory or numerical experiments) may lead to a clearer understanding of upwelling under spreading centres.

From this study we conclude that any spreading boundary in the world's ocean basins would exhibit an even and predictable segmentation. Evaluation on the proposed 30–85-km length scale of other existing spreading centre data, as well as additional high-resolution surveys of seafloor spreading boundaries are required to determine whether spreading-centre spacing is dependent only on spreading rate (indicating a uniform process of upwelling beneath ridges on a global scale) or whether a consistent spreading-centre spacing and consequent uniformity of mantle upwelling should be considered on the regional scale of individual plate boundaries, mantle plumes or other heterogeneities of the Earth's mantle.

We thank H. J. B. Dick, J. A. Karson, R. C. Kerr and G. M. Purdy for constructive criticism. This work was supported by the Office of Naval Research, Contract N00014-82-C-0019 and a grant from the Center for Analysis of Marine Systems (CAMS) of the Woods Hole Oceanographic Institution with funds from the Exxon Education Foundation. Pam Foster and Maureen Carragher processed the manuscript. Woods Hole Oceanographic Institution Contribution 5974.

Received 18 March; accepted 17 July 1985.

1. Schouten, H. & Klitgord, K. D. *Earth planet. Sci. Lett.* **59**, 255–266 (1982).
2. Schouten, H. & Klitgord, K. D. *Nature* **303**, 549–550 (1983).
3. Schouten, H. & White, R. S. *Geology* **8**, 175–179 (1980).
4. Detrick, R. S. & Purdy, G. M. *J. geophys. Res.* **85**, 3759–3777 (1980).
5. Detrick, R. S., Cormier, M. H., Prince, R. A., Forsyth, D. W. & Ambos, E. L. *J. geophys. Res.* 10599–10612 (1982).
6. Sinha, M. C. *EOS* **64**, 314 (1983) (abstr.).
7. Mutter, J. C. & Detrick, R. S. *Geology* **12**, 534–537 (1984).
8. Macdonald, K. C. & Fox, P. J. *Nature* **302**, 55–58 (1983).
9. Macdonald, K. C., Sempere, J.-C. & Fox, P. J. *J. geophys. Res.* **11**, 6049–6069 (1984).
10. Whitehead, J. A., Dick, H. J. B. & Schouten, H. *Nature* **312**, 146–148 (1984).
11. Howard, L. N. *Proc. 11th int. Congr. Appl. Mech.*, Munich, 1109–1115 (Springer, Berlin, 1966).
12. Lonsdale, P. *EOS* **63**, 1108 (1982).
13. Lonsdale, P. *J. geophys. Res.* **88**, 9393–9406 (1983).
14. Lonsdale, P., *Bull. geol. Soc. Am.* **96**, 313–327 (1985).
15. Ramberg, I. B. & van Andel, Tj. H. *Bull. geol. Soc. Am.* **88**, 577–586 (1977).
16. Rona, P. A., Harbison, R. N., Bussiner, B. G., Scott, R. B. & Natwalk, A. J. *Bull. geol. Soc. Am.* **87**, 661–674 (1976).
17. Rona, P. A. & Gray, D. F. *Bull. geol. Soc. Am.* **91**, 485–496 (1980).
18. Fox, P. J. & Gallo, D. G. *Tectonophysics* **104**, 205–242 (1984).
19. Karson, J. & Dick, H. J. B. *Mar. geophys. Res.* **6**, 51–98 (1983).
20. Ballard, R. D., van Andel, Tj. H. & Holcomb, R. T. *J. geophys. Res.* **87**, 1149–1161 (1982).
21. Francheteau, J. & Ballard, R. D. *Earth planet. Sci. Lett.* **64**, 93–116 (1983).
22. Lichtman, G. S. & Eissen, J. P. *Geology* **11**, 592–595 (1983).
23. Crane, K. *Earth planet. Sci. Lett.* **72**, 405–414 (1985).
24. Whitehead, J. A. & Luther, D. S. *J. geophys. Res.* **80**, 705–717 (1975).
25. Marsh, B. D. *J. Geol.* **87**, 687–713 (1979).
26. Bryan, W. B., Thompson, G., Frey, F. A. & Dickey, G. S. *J. geophys. Res.* **81**, 4285–4304 (1976).
27. Turcotte, D. L. & Schubert, G. *Geodynamics Applications of Continuum Physics to Geological Problems* (Wiley, New York, 1982).
28. Parker, R. L. & Oldenburg, D. W. *Nature Phys. Sci.* **242**, 137–139 (1973).
29. Klitgord, K. D. & Mammerickx, J. *J. geophys. Res.* **87**, 6725–6750 (1982).
30. Searle, R. C. *Geology* **11**, 607–610 (1983).
31. Palm, E. *Adv. appl. Mech.* **18**, 77–121 (1978).
32. Busse, F. M. *Adv. appl. Mech.* **18**, 77–121 (1978).
33. Scott, D. R. & Stevenson, D. J. *Geophys. Res. Lett.* **11**, 1161–1164 (1984).
34. Ballard, R. D. & van Andel, Tj. H. *Bull. geol. Soc. Am.* **88**, 507–530 (1977).
35. Collette, B. J., Verhoef, J. & Mulder, A. F. J. *J. Geophys.* **47**, 91–98 (1980).
36. Dick, H. J. B. & Sinton, J. M. *J. Geol.* **87**, 403–416 (1979).
37. Cooper, R. F. & Kohlstedt, D. L. *Tectonophysics* **107**, 207–233 (1984).
38. Minster, J. B. & Jordan, T. H. *J. geophys. Res.* **83**, 5331–5354 (1978).